Catalysis Today 144 (2009) 2–6

Contents lists available at ScienceDirect

Catalysis Today

journal homepage: www.elsevier.com/locate/cattod

Photocatalytic synthesis of Se nanoparticles using polyoxometalates

T. Triantis [a], A. Troupis [a], E. Gkika [a], G. Alexakos [a], N. Boukos [b], E. Papaconstantinou [a,*], A. Hiskia [a,**]

[a] Institute of Physical Chemistry, NCSR Demokritos, Neapoleos 73, 15310 Athens, Greece
[b] Institute of Materials Science, NCSR Demokritos, Neapoleos 73, 15310 Athens, Greece

ARTICLE INFO

Article history:
Available online 6 February 2009

Keywords:
Polyoxometalates
Nanostructures
Selenium nanoparticles
Size-control

ABSTRACT

Selenium nanoparticles are formed upon photolysis of solutions of (propan-2-ol/POM/Se(IV)), where polyoxometalate (POM) is either $PW_{12}O_{40}^{3-}$ or $SiW_{12}O_{40}^{4-}$. Propan-2-ol serves as sacrificial reagent for the photoformation of 1-equivalent reduced blue polyoxometalate, POM(e), which further reacts with Se(IV) to produce selenium nanoparticles. POM serves both as relay for the transfer of electrons from propan-2-ol to Se(IV) and stabilizer for the nanoparticles. Changing the ionic strength from 0 to 0.025 and 0.05 M, results in the formation of gradually larger nanoparticles 40, 60 and 90 nm, respectively. Increase of the initial concentration of $SiW_{12}O_{40}^{4-}$, from 2 to 4 and 10×10^{-3} M, results in the formation of gradually smaller nanoparticles, 110, 80 and 60 nm, respectively.

1. Introduction

Polyoxometalate (POM) anions include a large variety of oxygen bridged metal clusters well known for their unique redox chemistry, characterized by their ability to accept and release a certain number of electrons, in distinct steps, without decomposition [1–3].

Under irradiation at the $O \rightarrow M$ charge transfer band (near visible and UV region), POM become powerful oxidants for a great variety of organic compounds, including organic pollutants [4,5]. The reduced form of POM, is a powerful reducing reagent, which can be easily reoxidised by a diverse number of chemicals [6] including metal ions, i.e. Ag^{+}, Cu^{2+}, Pd^{2+}, Au^{3+}, Hg^{2+} or Cr^{6+}, resulting in closing the photocatalytic cycle, according to the following reactions [7]

$$POM + S \xrightarrow{hv} POM(e^{-}) + S_{ox} \quad (1)$$

$$POM\,(e^{-}) + M^{n+} \rightarrow POM + M^{0} \quad (2)$$

Recently it has been presented that, by adjusting the conditions at low ionic strength, synthesis of Ag, Pd, Au and Pt metal nanoparticles with reasonably small size distribution can be achieved (Reaction (3); M^{0}_{coll} = colloidal metal) [8]

$$POM\,(e^{-}) + M^{n+} \rightarrow POM + M^{0}_{coll} \quad (3)$$

Reactions (1) and (3) may be separated in time and space (two pots system), or occur in a one pot system, where POM play the double role of photocatalytic reducing reagent and stabilizer. The method is simple and efficient in ambient temperature, taking place within a few seconds, and has been advanced to the synthesis of other nanostructured materials, such as bimetallic nanoparticles, nanosheets or nanorings [9].

Nanometer scale materials are of intriguing interest due to their photocatalytic, photovoltaic and optoelectronic properties [10], their catalytic role in various chemical reactions [11] and even their antiseptic ability [12]. Since these properties are a function of the size of the dispersed metal particles, the establishment of methods with which one could control and select the size of the produced particles is of paramount interest in order to maximize the efficiency of the particles [13–15].

Selenium has been important in a wide variety of applications that range from photocells, photographic exposure meters and solar cells to semiconductor rectifiers [16]. So far, various methods have been reported on the synthesis of selenium nanostructures including chemical reduction [17,18], radiolytic [19] and sonochemical methods [20], by using various reagents but only very few of them deal with size control of the Se nanoparticles [21,22].

In this study, the photocatalytic reduction of Se(IV) and the formation of colloidal solution of nanospheres of Se^{0}, in the presence of $SiW_{12}O_{40}^{4-}$ and $PW_{12}O_{40}^{3-}$, are presented. The influence of various parameters such as nature of POM, concentration of reactants and ionic strength on thermal reaction (3) has been investigated as well as their effect on the size of Se nanoparticles. It should be noted that during the course of the investigation, another paper, along these lines, has recently appeared in the literature dealing with synthesis of Se nanoparticles using $H_4SiW_{12}O_{40}$ [22]. Our study, besides verifying literature results [22], reports that size controlled Se^{0} nanoparticles can be further achieved by changing POM initial concentration and/or ionic strength.

* Corresponding author.
** Corresponding author. Fax: +30 2106511766.
E-mail address: hiskia@chem.demokritos.gr (A. Hiskia).

0920-5861/$ – see front matter © 2009 Elsevier B.V. All rights reserved.
doi:10.1016/j.cattod.2008.12.028

2. Experimental

2.1. Materials

Na_2SeO_3 (95%) was obtained from Acros Organics. $H_4SiW_{12}O_{40}$ (99.9+%) and $H_3PW_{12}O_{40}$ was purchased from Aldrich and Riedel-de Haen, respectively and used as received. $NaClO_4$ (99%) was obtained from Aldrich. Propan-2-ol was analytical grade. All of the other chemicals are of reagent grade. Ultra pure water was obtained from a compact apparatus from Barnstead. Extra pure nitrogen (99.999%) and dioxygen (>99.95%) were used for deaeration or oxygenation of solutions.

2.2. Synthesis of Se nanoparticles

A typical experiment in which reactions (1) and (3) proceed separately is as follows: 4 ml of an aqueous solution of POM (7×10^{-4} M) and propan 2-ol (0.5 M), were placed into a spectrophotometer cell (1 cm path length), deaerated with N_2 and then covered with a serum cap. pH was set at 1, 2.5 and 5 only for $SiW_{12}O_{40}^{4-}$, as $PW_{12}O_{40}^{3-}$ is stable only around pH 1. Acidification of the solutions was done, whenever necessary, with $HClO_4$. The ionic strength was adjusted using $NaClO_4$ at various concentrations (0–0.1 M).

Upon illumination the solution turned blue due to the formation of reduced POM, POM(e^-), reaction (1). Photolysis was performed with an Oriel 1000-W Xe arc lamp equipped with a cool water circulating filter to absorb the near-IR radiation and a 320-nm cutoff filter in order to avoid direct photolysis of organic substrates. The incident radiation was reduced to ~40% with a slit diaphragm in order to obtain reasonable photolysis times. The total photonic flux (320–345 nm) determined by ferrioxalate actinometry was 7.9×10^{-6} einstein min^{-1}.

The degree of reduction of POM in photolyzed deaerated solutions was calculated from the known molar absorption coefficient of the 1-equiv-reduced 12-tungstophosphate, $PW_{12}O_{40}^{4-}$ (ε_{752} = 1600 M^{-1} cm^{-1}) and 1-equiv-reduced 12-tungstosilicate, $SiW_{12}O_{40}^{5-}$ (ε_{730} = 2100 M^{-1} cm^{-1}), using a PerkinElmer Lambda 19 spectrophotometer [23].

In turn, in the absence of light, Se nanoparticles were obtained by injecting a deaerated concentrated aqueous solution of Na_2SeO_3 (few μl were added in order to obtain concentration of Se(IV) ions of ca 1.5×10^{-4} M) to the already prepared POM(e^-) solution (4 ml), which remains sealed with the serum cap. The solutions were mixed, agitated for ca 3 s and allowed to stand.

The initial rate of POM(e^-) reoxidation was calculated by the slope of the curve of the concentration of POM(e^-) vs. time of the reaction with Se(IV) ions, for conversion less than 30%.

Alternatively, Se^0 nanoparticles were obtained in one pot system by mixing from the beginning the POM and Se(IV) solutions prior to photolysis step.

2.3. Characterization of Se nanoparticles

The obtained Se nanoparticles were characterized using Transmission Electron Microscopy. TEM images were obtained using an FEI 200 kV microscope equipped with a GIF 200 Gatan imaging filter utilized for Energy Filtered Transmission Electron Microscopy. TEM samples were prepared by placing microdrops of colloid solution on a carbon coated copper grid. The subsequent analysis for the size distribution of the particles was based on the counting of ca. 150 particles.

Indication of formation of Se nanoparticles was also noticed from the spectra of the colloid solution, attributed to the plasmon-resonance absorbance of these nanoparticles. Experimental details are described in the corresponding figures.

3. Results and discussion

3.1. Thermal redox reactions between reduced POM and Se(IV) and synthesis of Se^0 nanoparticles

Deaerated solutions of 1-equivalent-reduced blue tungstates, $PW_{12}O_{40}^{4-}$ or $SiW_{12}O_{40}^{5-}$ ~6×10^{-4} M, are produced upon photolysis of aqueous solutions of 7×10^{-4} M POM, 0.5 M propan-2-ol. The pH varied from 1 (for $PW_{12}O_{40}^{3-}$ and $SiW_{12}O_{40}^{4-}$) to 2.5 (for $SiW_{12}O_{40}^{4-}$) and 5 (for $SiW_{12}O_{40}^{4-}$). These solutions are mixed with a deaerated concentrated aqueous solution of Na_2SeO_3 to a final concentration of Se(IV) ions of ca 1.5×10^{-4} M. The process of this thermal reaction (3) is monitored at 752 and 730 nm, for the 1-equivalent-reduced $PW_{12}O_{40}^{4-}$ and $SiW_{12}O_{40}^{5-}$, respectively. The blue colour of reduced POM(e^-) rapidly disappears (Fig. 1) indicating fast reoxidation of reduced POM(e^-) by Se(IV) ions. For $SiW_{12}O_{40}^{5-}$ the initial rates of reoxidation are 12.8, 8.8 and 5.2×10^{-4} M min^{-1} for pH 1, 2.5 and 5, respectively. Since the redox potential of used POM [$E^0(SiW_{12}O_{40}^{4-}/SiW_{12}O_{40}^{5-})$ = 0.057 V vs. NHE] is independent of pH [4,24], these results may be attributed to the decrease of selenium potential, [E^0(Se(IV)/Se^0) = 0.778 V], with increasing of pH [25].

Different rates are also observed by using different POM. $SiW_{12}O_{40}^{5-}$ with a more negative (or, rather, "less positive") redox potential [$E^0(SiW_{12}O_{40}^{4-}/SiW_{12}O_{40}^{5-})$ = 0.057 V vs. NHE] reacts an order of magnitude faster with Se(IV) than 12-tungstophosphate [$E^0(PW_{12}O_{40}^{3-}/PW_{12}O_{40}^{4-})$ = 0.221 V vs. NHE] [4,24].

When the reaction is over, a ratio [$SiW_{12}O_{40}^{5-}$]/[Se(IV)] = 4:1, for pH 1 and 2.5, is marked. However, for $SiW_{12}O_{40}^{5-}$ at pH 5 and in experiments with $PW_{12}O_{40}^{4-}$ (pH 1), the ratio [POM(e^-)]/[Se(IV)] is 3:1. In addition, the blue remaining colour of the solution indicates partial reoxidation of POM(e^-) by Se(IV). This may be explained by the diminishing of the redox potential differences of the reactants that prevents thermal reaction (3) to go to completion. For instance, at pH 1 $PW_{12}O_{40}^{4-}$ is worst reductant than $SiW_{12}O_{40}^{5-}$, whereas, at pH 5 selenium becomes worst oxidant than at pH 1 [25]. This conclusion is in agreement with the fact that Se(I) does not seem to exist under these conditions and besides Se^0 nanoparticles are identified in these solutions, as shown below.

Fig. 2 shows the initial spectra of reduced blue $SiW_{12}O_{40}^{5-}$ and the resulting spectra of Se nanoparticles. No precipitation of Se^0 is observed. The solution turns from the initially blue colour of

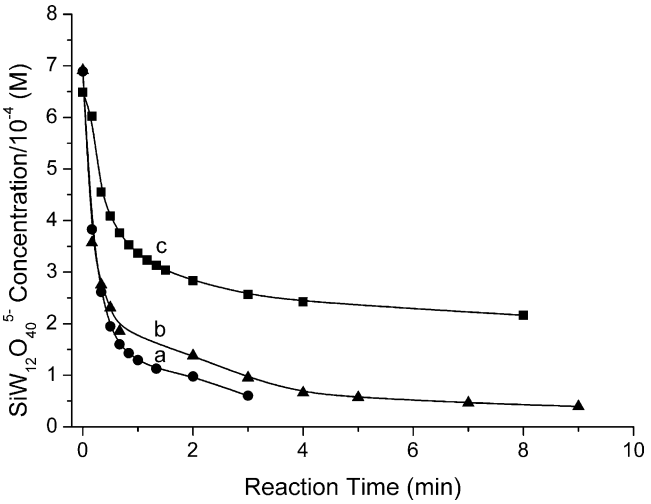

Fig. 1. Thermal reoxidation of $SiW_{12}O_{40}^{5-}$ ~6×10^{-4} M by Se(IV) 1.5×10^{-4} M after photolysis of deaerated aqueous solutions of $SiW_{12}O_{40}^{4-}$ 7×10^{-4} M, propan-2-ol 0.5 M at (a) pH 1, (b) 2.5 and (c) 5.

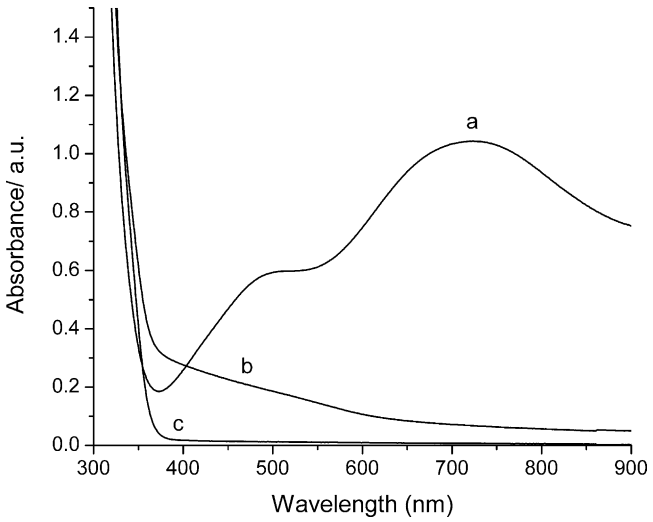

Fig. 2. Absorption spectra showing (a) the 1-equivalent reduced POM $SiW_{12}O_{40}^{5-}$ after photolysis of deaerated aqueous solutions of $SiW_{12}O_{40}^{4-}$ 7×10^{-4} M, propan-2-ol 0.5 M, pH 1, (b) the formation of Se^0 nanoparticles upon mixing solution (a) with Se(IV) to final concentration of 1.5×10^{-4} M and (c) the oxidized form of POM $SiW_{12}O_{40}^{4-}$ prior to photolysis.

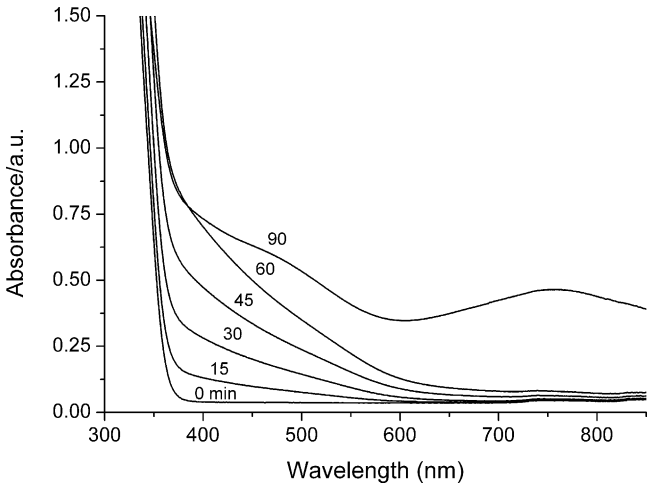

Fig. 3. Gradual development of the orange-red colour, characteristic of selenium nanoparticle absorbance, upon photolysis of a deaerated $SiW_{12}O_{40}^{4-}$ 7×10^{-4} M/propan-2-ol 2 M/Se(IV) 7×10^{-4} M aqueous solution at pH 5.

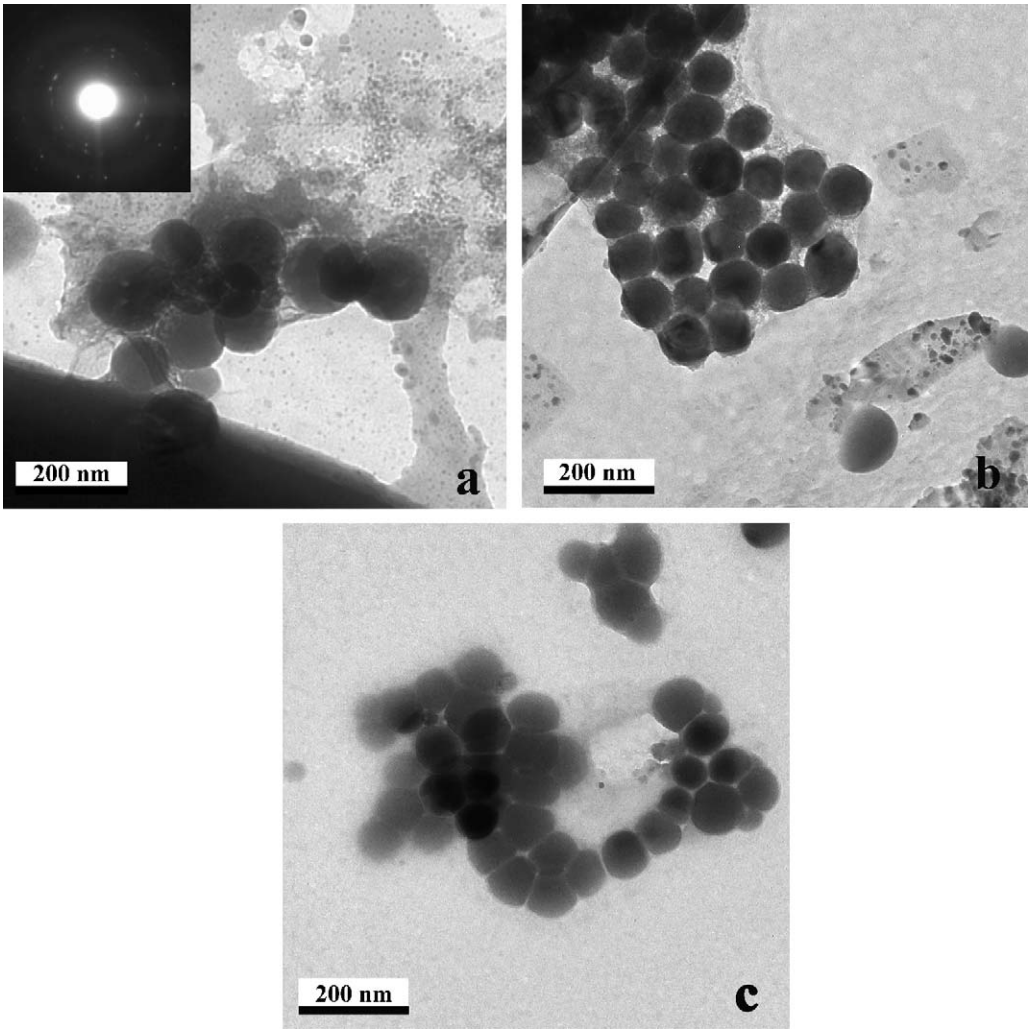

Fig. 4. TEM images of selenium nanoparticles obtained upon reduction of Se(IV) 1×10^{-3} M by various concentrations of $SiW_{12}O_{40}^{4-}$ (a) 2×10^{-3} M, (b) 4×10^{-3} M and (c) 10×10^{-3} M. The inset is the corresponding selected area electron diffraction pattern.

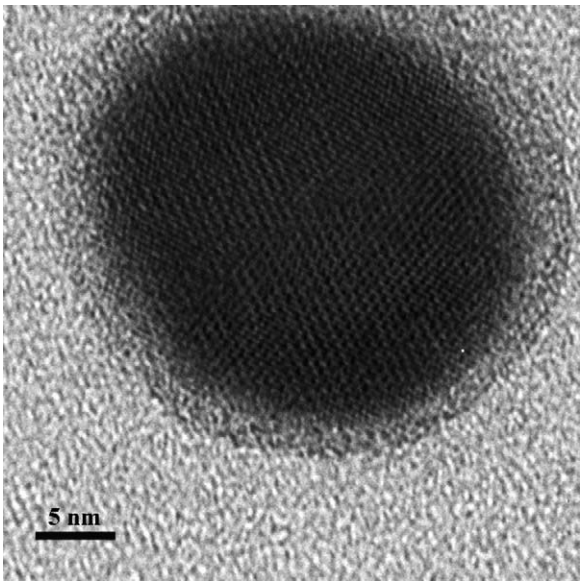

Fig. 5. HRTEM image of a Se^0 nanoparticle obtained upon reduction of Se(IV) 1×10^{-4} M by $SiW_{12}O_{40}^{5-}$ 10^{-3} M (propan-2-ol 1 M, pH 1).

reduced POM(e^-) to the orange-red colour assigned to plasmon resonance of Se nanoparticles. It was observed that under these conditions the suspensions of Se^0 nanoparticles are stable for months.

These results have been obtained through the separation of the photochemical from the thermal reaction. However, combinations of both in one pot experiments have also been performed for the synthesis of Se^0 nanoparticles. Fig. 3 shows the gradual development of the orange-red colour, characteristic of selenium nanoparticle absorbance, upon photolysis of a deaerated ($SiW_{12}O_{40}^{4-}$/propan-2-ol/Se(IV)) aqueous solution. Similar results have also been obtained using deaerated ($PW_{12}O_{40}^{3-}$/propan-2-ol/Se(IV)) aqueous solution.

3.2. Size-controlled synthesis of Se^0 nanoparticles

3.2.1. Influence of $SiW_{12}O_{40}^{4-}$ initial concentration

Upon photolysis of solutions of ($SiW_{12}O_{40}^{4-}$/propan-2-ol/Se(IV)), in which POM concentrations vary and Se(IV) initial concentration is always 1×10^{-4} M, different sizes of Se nanoparticles are obtained.

The TEM images of the produced Se^0 nanoparticles are shown in Fig. 4, while the inset in Fig. 4a is the corresponding selected area electron diffraction pattern indicating the crystallinity of the Se nanoparticles. Increase of the initial concentration of $SiW_{12}O_{40}^{4-}$, from 2 to 4 and finally to 10×10^{-3} M, results in the formation of gradually smaller nanoparticles. Their size ranges from to 110 to 80 and finally to 60 nm, respectively. The fact that smaller Se^0 nanoparticles are formed with increasing of the initial concentration of $SiW_{12}O_{40}^{4-}$ implies that the nucleation process is enhanced more than the growth of Se^0 nanoparticles.

Fig. 5 is a representative high resolution transmission electron microscopy (HRTEM) image of one Se^0 crystal nanoparticle produced upon photolysis of ($SiW_{12}O_{40}^{4-}$ 5×10^{-3} M/propa-2-ol 1 M) to form one-equivalent tungstate, $SiW_{12}O_{40}^{5-}$ 1×10^{-3} M and addition of Se(IV) 1×10^{-4} M. An amorphous shell, 1–3 nm thick, surrounds the Se crystalline core. This shell was studied by energy filtered transmission electron microscopy (EFTEM). Fig. 6a shows a bright field micrograph of the Se^0 nanoparticle, while Fig. 6b–e are the Se, O, Si and W EFTEM images, respectively. The EFTEM images represent elemental maps, where a bright area indicates a high elemental concentration. These images are evidence that the core of the nanoparticles is Se, while the surrounding shell is composed of O, Si and W, that is, POM. These results verify our previous studies according to which POM serve as both reducing reagents and stabilizers in synthesis of metal nanoparticles [8,26,27].

According to our previous studies, control of the size of the particles can be also achieved via rate control of reaction (3). Faster reduction of metal ion leads to smaller and more uniform nanoparticles suggesting that the rate of metal ion reduction affects strongly the initial nucleation of particles. A way for this to

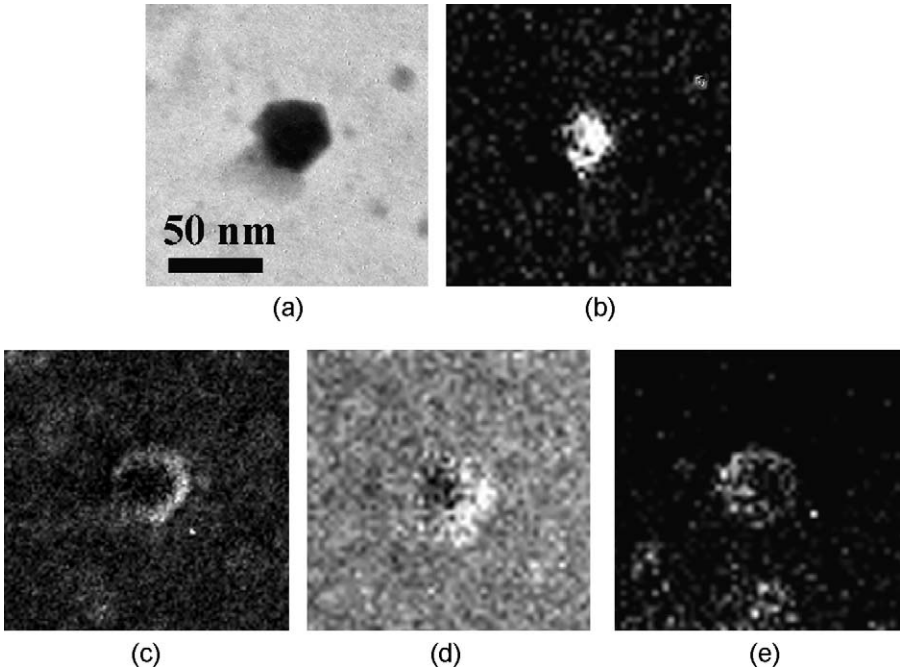

Fig. 6. (a) Bright field image and (b) Se, (c) O, (d) Si and (e) W EFTEM images of a Se^0 nanoparticle.

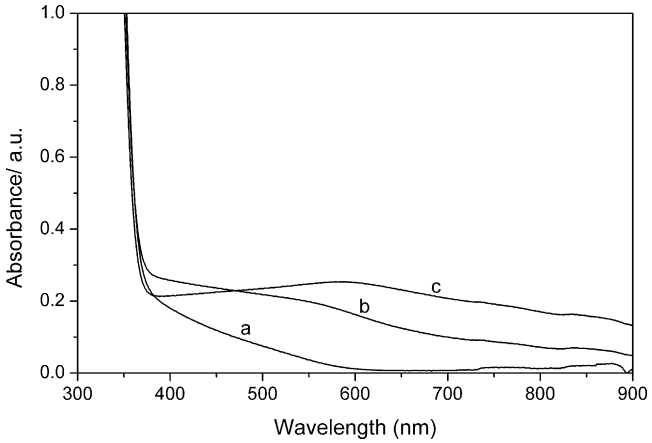

Fig. 7. Absorption spectra obtained by varying the ionic strength of the solution containing $SiW_{12}O_{40}^{4-}$ 4×10^{-3} M, propan-2-ol 2 M and Se(IV) 1×10^{-3} M, pH 5. [$NaClO_4$] is (a) 0, (b) 0.025 and (c) 0.05 M.

be achieved is by increasing the concentration of the reducing reagent (reduced POM). Alternatively, the concentration of metal ions also influences the size of the obtained particles, that is, larger concentrations of metal ions form larger nanoparticles [26]. In this respect two series of preliminary experiments were performed by changing (a) the initial $SiW_{12}O_{40}^{5-}$ concentration from 5 to 7.7 and finally to 10×10^{-4} M keeping the initial concentration of Se(IV) constant (1×10^{-4} M) and (b) by changing the initial concentration of Se(IV) from 0.5 to 1 and finally to 1.5×10^{-3} M keeping the initial concentration of POM constant, 2×10^{-3} M. In both set of experiments, size control of Se^0 nanoparticles was not achieved. The size of Se^0 nanoparticles had mean diameter 27 ± 3 nm. It turned out that the differences in the rates of the reactions, in both set of experiments, were too small to affect the size of Se nanoparticles.

3.2.2. Influence of ionic strength

Different sizes of Se nanoparticles are also obtained by varying the ionic strength of solutions using different concentrations of $NaClO_4$. Experiments were carried out in aqueous solution containing $SiW_{12}O_{40}^{4-}$, (4×10^{-3} M), propan 2-ol (2 M) and Se(IV) (1×10^{-3} M). pH was set at ca 5 without adjustment and $NaClO_4$ concentration was ranged from 0 to 0.1 M. It was observed that upon increasing $NaClO_4$ concentration the size of Se^0 nanoparticles was also increased. Increase of the concentration of $NaClO_4$, from 0 to 0.025 and finally to 0.05 M, results in the formation of gradually larger nanoparticles. Their size is ranged from to 40 to 60 and finally to 90 nm, respectively. When $NaClO_4$ concentration was set at 0.1 M or more, deposition of Se^0 took place. The precipitate produced was of reddish colour, characteristic of selenium zero-state particles.

The size control of Se^0 nanoparticles, achieved in the above experiments, can also be monitored by UV–vis spectrophotometry. Fig. 7 shows the absorption spectra of the suspensions of selenium nanoparticles for different $NaClO_4$ concentrations. A red-shift in the absorption spectra of these particles is observed as the particle sizes increase. This trend in the absorption spectra has also been reported by others [21]. A first approach to these results is that, in these experiments, there is a sequence of reactions going on: the photochemical reaction (1) followed by the thermal reaction (2). The rate of reaction (1) which involves an excited negatively charged POM and a neutral molecule, should be rather unaffected by the change in ionic strength of the solution. On the other hand, thermal reaction (2) involves two negatively charged species, POM(e^-) and SeO_3^{2-} and, as known, increase in ionic strength should increase the rate of this reaction. This, for selenium, favors growth rather than nucleation, contrary to what has been observed so far for silver nanoparticles [26]. In this case, besides the fact that there is a multiple reduction of Se(IV) to reach Se^0, the presence of $NaClO_4$, most likely, interferes with the stabilization of selenium particles by POM, in the early stages of nucleation, thus favoring growth rather than nucleation.

4. Conclusions

A simple method for making selenium nanoparticles involves photolysis of a deaerated solution of (propan-2-ol/POM/Se(IV)). POM serves as reducing reagent, as well as stabilizer for the particles as EFTEM images have shown. Size control of the particles has been achieved, so far, by changing the concentration of POM and the ionic strength of the solutions.

Acknowledgements

T. Triantis and A. Troupis are grateful to NCSR Demokritos, Institute of Physical Chemistry, for postdoctoral fellowships.

References

[1] M.T. Pope, Heteropoly and Isopoly Oxometalates, Springer-Verlag, Berlin, 1983, p. 1.
[2] M.T. Pope, A. Muller, Angew. Chem. Int. Ed. 30 (1991) 34.
[3] V.W. Day, W.G. Klemperer, Science 228 (1985) 533.
[4] E. Papaconstantinou, Chem. Soc. Rev. 16 (1989) 1.
[5] A. Hiskia, A. Mylonas, E. Papaconstantinou, Chem. Soc. Rev. 30 (2001) 62.
[6] A. Hiskia, E. Papaconstantinou, Inorg. Chem. 31 (1992) 163.
[7] E. Gkika, A. Troupis, A. Hiskia, E. Papaconstantinou, Environ. Sci. Technol. 39 (2005) 4242, and references therein.
[8] A. Troupis, A. Hiskia, E. Papaconstantinou, Angew. Chem. Int. Ed. 41 (2002) 1911.
[9] S. Mandal, P.R. Selvakannan, R. Pasricha, M. Sastry, J. Am. Chem. Soc. 125 (2003) 8440.
[10] V. Subramanian, E.E. Wolf, P.V. Kamat, Langmuir 19 (2003) 469.
[11] L.M. Liz-Marzán, P.V. Kamat, in: L.M. Liz-Marzán, P.V. Kamat (Eds.), Nanoscale Materials, Kluwer Academic Publishers, Boston/Dordrecht/London, 2003, , p. 1, chapter 1.
[12] G.A. Martinez-Castanon, N. Niño-Martínez, F. Martínez-Gutierrez, J.R. Martínez-Mendoza, F. Ruiz, J. Nanopart. Res. 10 (2008) 1343.
[13] Y. Song, Y. Yang, C.J. Medforth, E. Pereira, A.K. Singh, H. Xu, Y. Jiang, C.J. Brinker, F. Swol, J.A. Shelnutt, J. Am. Chem. Soc. 126 (2004) 635.
[14] Z.S. Pillai, P.V. Kamat, J. Phys. Chem. B 108 (2004) 945.
[15] M.A. Watzky, R.G. Finke, Chem. Mater. 9 (1997) 3083.
[16] E. Best, I. Hinz, H. Wendt, Selen, in: K.H. Kugler (Ed.), Gmelin Handbuch der Anorganischen Chemie, vol. 10, Springer, Berlin, 1979, p. 168.
[17] J.S. Zhang, H.L. Wang, Y.P. Bao, L.D. Zhang, Life Sci. 75 (2004) 237.
[18] N.M. Dimitrijevic, P.V. Kamat, Langmuir 4 (1988) 782.
[19] Y. Zhu, Y. Qian, H. Huang, M. Zhang, Mater. Lett. 28 (1996) 119.
[20] X. Wang, X. Zheng, J. lu, Y. Xie, Ultrason. Sonochem. 11 (2004) 307.
[21] Z.-H. Lin, C.R. Chris Wang, Mater. Chem. Phys. 92 (2005) 591.
[22] L.B. Yang, Y.H. Shen, A.J. Xie, J.J. Liang, B.C. Zhang, Mater. Res. Bull. 43 (2008) 572.
[23] G.M. Varga Jr., E. Papaconstantinou, M.T. Pope, Inorg. Chem. 9 (1970) 662.
[24] M.T. Pope, G.M. Varga, Inorg. Chem. 5 (1966) 1249.
[25] S. Sanuki, T. Kojima, K. Arai, S. Nagaoka, H. Majima, Metall. Mater. Trans. B 30 (1999) 15.
[26] A. Troupis, T. Triantis, A. Hiskia, E. Papaconstantinou, Eur. J. Inorg. Chem. (2008) 5579.
[27] A. Hiskia, E. Papaconstantinou, A. Troupis, International Patent PCT/GR 2004/0049, WO2006/038045 A1, 2006.